FORMOSAT-7/COSMIC-2
Space Weather Data Release 5

March 16, 2022

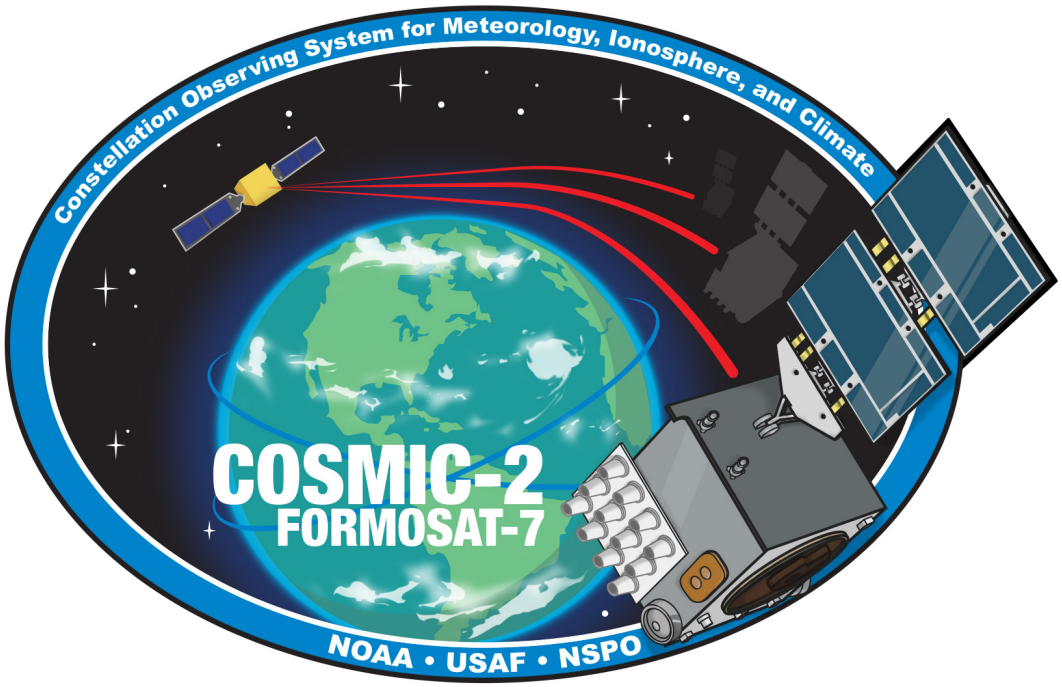

Submitted by:

DocuSigned by:
Paul Straus
5F3C366C7EA74E5...

3/18/2022

Dr. Paul Straus
FORMOSAT-7/COSMIC-2 Space Weather Cal/Val Lead
The Aerospace Corporation

Concurred by:

DocuSigned by:
Dr. William Schreiner
ABD906434F1D405...

3/21/2022

Dr. William Schreiner
FORMOSAT-7/COSMIC-2 Mission Scientist
Director, COSMIC Program
University Corporation for Atmospheric Research

Concurred by:

DocuSigned by:
Capt. Ian Wheeler
3B9D2573D895419...

3/21/2022

Capt. Ian Wheeler
FORMOSAT-7/COSMIC-2 Payload Mission Manager
United States Space Force

Approved by:

DocuSigned by:
Dr. Elsayed Talaat
261D5FF664FA454...

3/21/2022

Dr. Elsayed Talaat
Director, Office of Projects, Planning, and Analysis
National Environmental Satellite, Data, and Information Service
National Oceanic and Atmospheric Administration

Approved by:

DocuSigned by:
Dr. Jong-Shinn Wu
75B65D439FD843C...

3/25/2022

Dr. Jong-Shinn Wu
Director General
National Space Organization

1 Background

The United States Air Force (USAF) Space Test Program launched six FORMOSAT-7/ COSMIC-2 (F7C2) satellites into a 24° inclination low Earth orbit on June 25, 2019. The primary F7C2 mission objective is to collect atmospheric and ionospheric data continuously as inputs into to daily near-real-time weather forecasts, climate studies, and space weather monitoring and forecasting. Each F7C2 satellite has three payloads. The primary instrument is the Tri-GNSS Radio-occultation System (TGRS) payload. Secondary instruments include the Ion Velocity Meter (IVM), andRadio Frequency Beacon (RFB) science payloads. Following spacecraft system activation and checkout, the primary and science payloads were first activated on July 16, 2019.

The F7C2 Space Weather Calibration/Validation (Cal/Val) effort is led by the United States Space Force (USSF) and assisted by experts from The Aerospace Corporation (AERO), Central Weather Bureau (CWB), Jet Propulsion Laboratory (JPL), National Cheng Kung University (NCKU), National Central University (NCU), National Oceanic and Atmospheric Administration (NOAA), National Space Organization (NSPO), the University Corporation for Atmospheric Research (UCAR), Boston College (BC), Utah State University (USU), Space Dynamics Laboratory (SDL), the Air Force Research Laboratory and the University of Texas at Dallas (UTD). Summaries of space weather early orbit and Cal/Val activities are described in [1] and [2].

This is the fifth data release pertaining to space weather data products. Previous releases provided relative Total Electron Content (TEC), electron density profiles and provisional scintillation amplitude index (S4) calculations made on-board by TGRS [4], absolute GPS TEC [5], absolute GLONASS TEC [6], and in-situ IVM density [7]. This data release provides TGRS observations of high-rate GNSS signal phase and amplitude associated with occultations that exhibit elevated amplitude scintillation, as well as S4 and scintillation phase ($\sigma\phi$) indices calculated from these high-rate data. Ancillary information that indicates when the high-rate data and scintillation indices are affected by ground-based Radio Frequency Interference (RFI) are also provided. Finally, this data release includes IVM in-situ ion temperature and composition data and provisional IVM ion drift products from the FM1 spacecraft between August 2019 and June 2020. FM1 was the first of the six F7C2 spacecraft lowered to 550 km altitude at which IVM is able to produce drift products.

2 Summary and Justification of Data Release

2.1 TGRS High-Rate Scintillation Observations

TGRS calculates an on-board S4 index at a 10 second cadence for every GNSS satellite it tracks via its precise orbit determination (POD) antennas. The time history of the S4 index is evaluated for every ionospheric occultation observed by TGRS. If the S4 index exceeds a configurable threshold at any point within an occultation, TGRS includes high-rate (50Hz for GPS/100Hz for GLONASS) phase and amplitude data for the occultation in its telemetry. Each ionospheric occultation generally extends over a range of tangent point altitudes from 90 km up to the spacecraft altitude. These high-rate scintillation data are provided in scnPhs files. An example of high-rate data collected by the TGRS is shown in Figure 1.

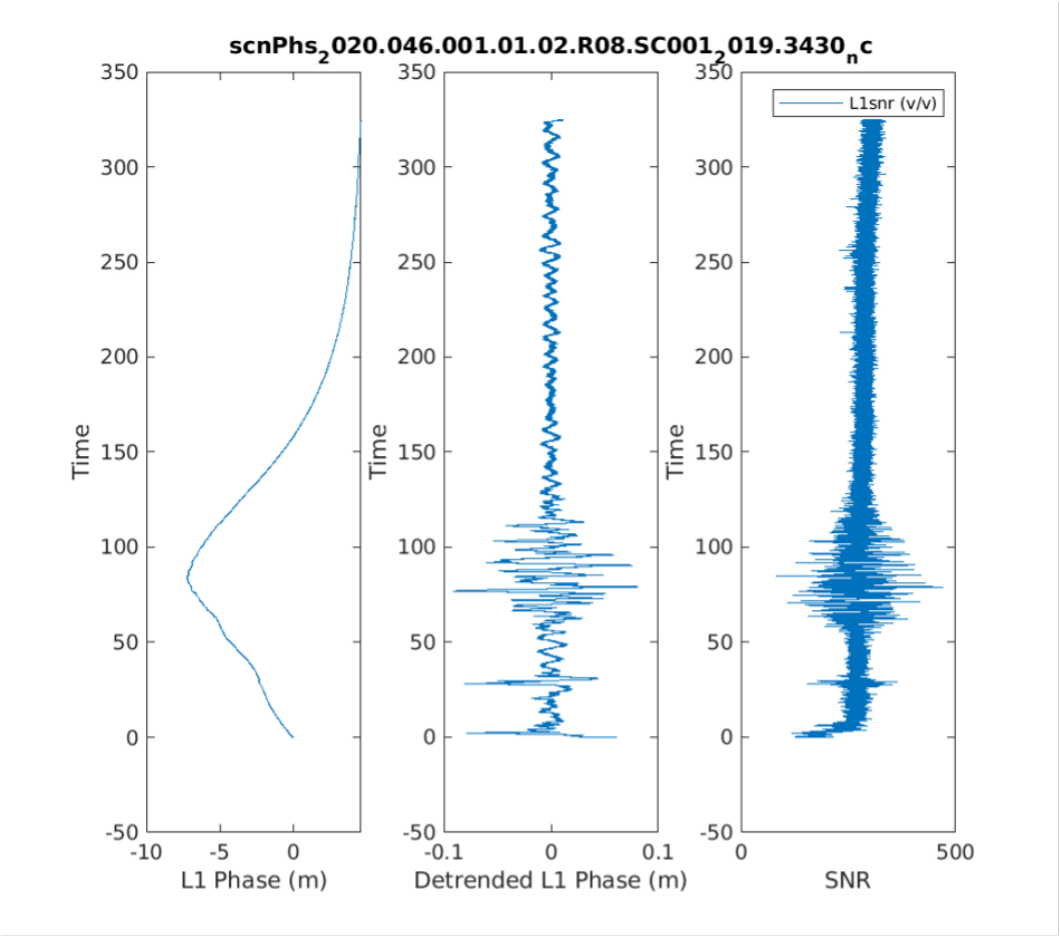

Figure 1: Example phase and amplitude data. Excess L1 phase (left), detrended L1 phase (center) and amplitude (ie SNR) observations (right) are displayed.

The demonstration of release readiness for L1 high-rate observations is based upon their successful use to geolocate ionospheric irregularity regions using back-propagation analysis.

The resulting geolocations were compared to far ultraviolet imagery from NASA's GOLD instrument, showing a strong correlation between plasma depletions that GOLD is sensitive to and the F7C2 irregularity region geolocations. An example of this type of analysis is provided in Figure 2. Release readiness for L2 high-rate observations is based upon consistency between geolocations determined from L1 and L2 data as shown in Figure 3. The zonal differences in Figure 3 indicate that the L1 and L2 geolocation results identify similar ionosphere irregularity regions as a function of longitude.

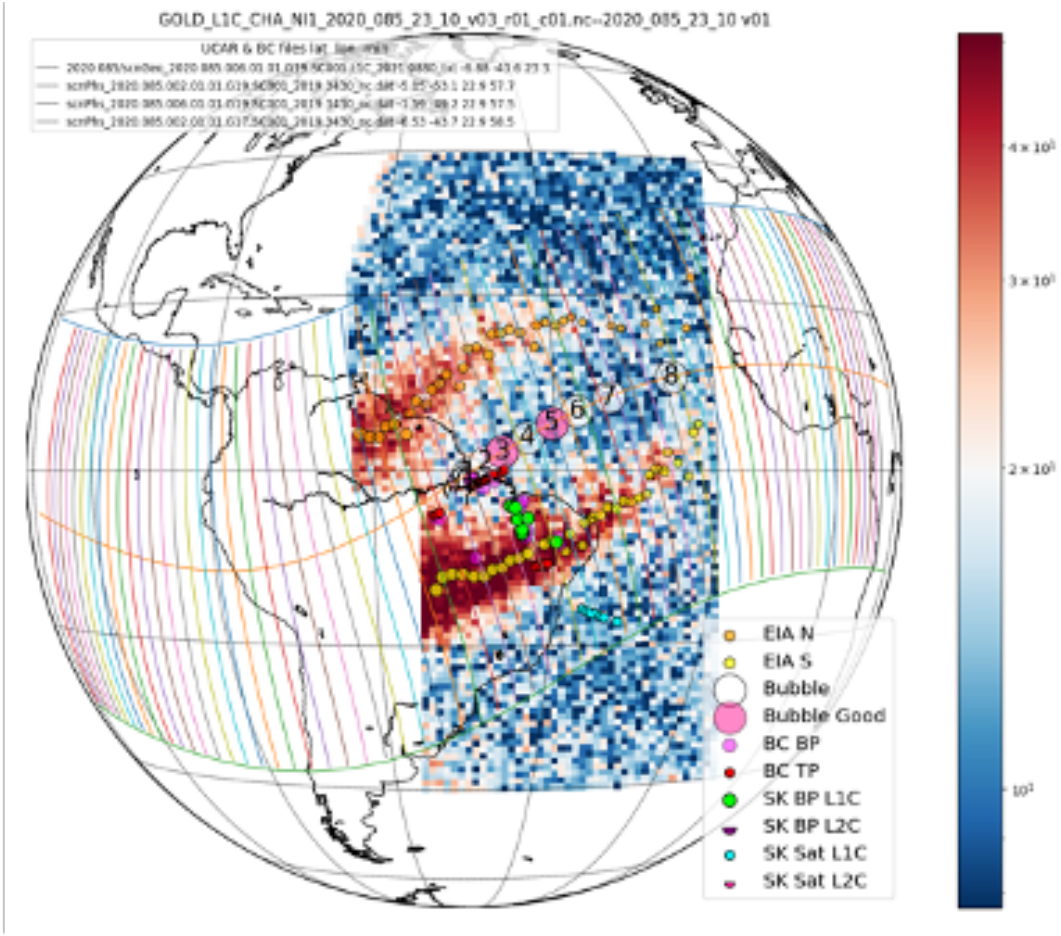

Figure 2: GOLD UV image showing equatorial bubbles (white and pink circles on magnetic equator) with scintillation geolocation results (green circles). TGRS scintillation geolocation has been compared to ionospheric irregularities from GOLD for verification.

The high-rate scintillation data being released is associated with TGRS flight software V4.3.4 (uploaded to F7C2 spacecraft in February and March 2020) and later versions. Data collected prior to TGRS V4.3.4 have not been verified, but may be released in the future.

High-rate phase and amplitude data collected by the TGRS are also processed into S4 and $\sigma\phi$ scintillation indice products. These two scintillation indices are computed using a sliding window of 10 seconds of data but are output at 1-second intervals. These products

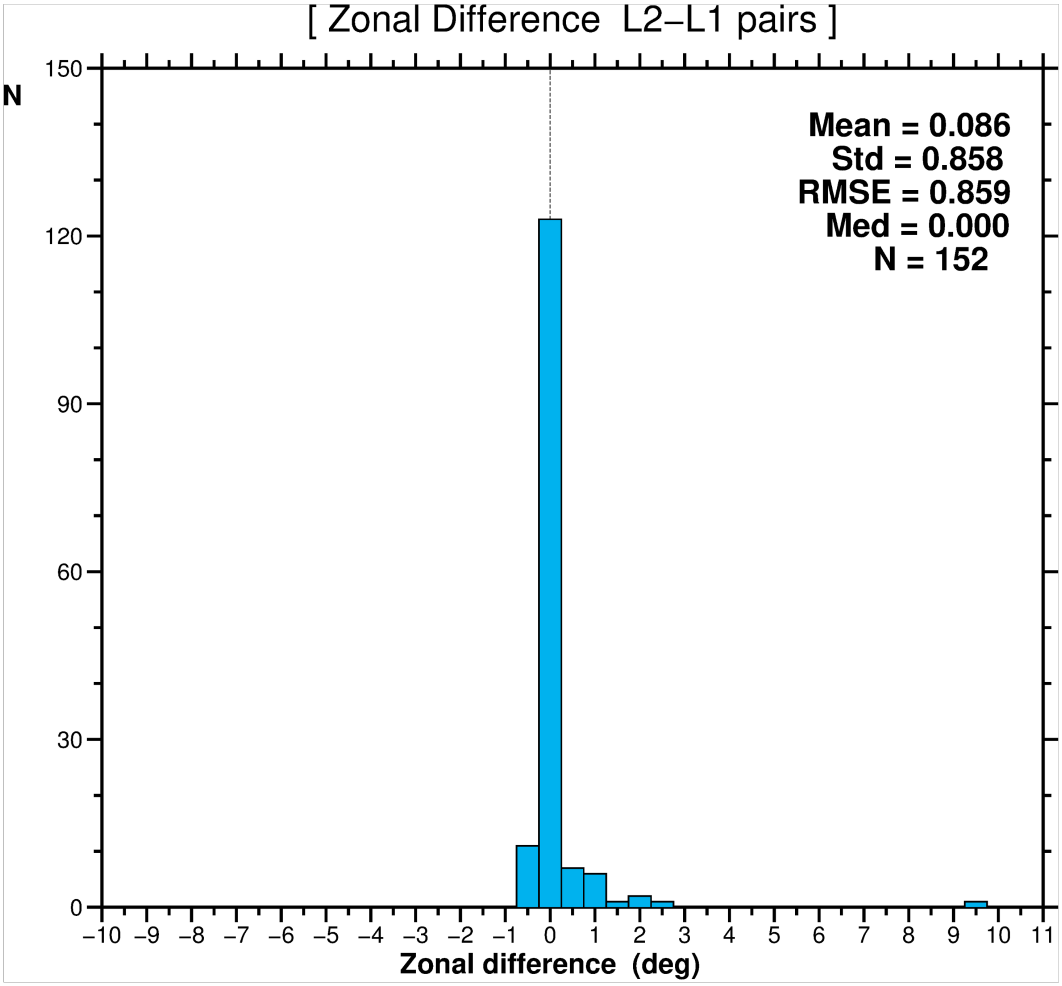

Figure 3: Zonal differences in scintillation geolocation pairs using L1 and L2 high-rate data.

are available as scnLv2 files (see Table 1) and only available when the on-board S4 index exceeds the configurable threshold described above. This high-rate data is used to compute the S4 and $\sigma\phi$ products contained in scnPhs files that are also provided as part of this release.

RFI can distort TGRS Signal-to-Noise Ratio (SNR) data and result in spurious S4 levels. RFI can be identified as present because it simultaneously affects the tracking of all GNSS satellites through a single POD antenna. Specifically, coherent SNR fluctuations with periods on the order of 10-20 seconds are observed. An algorithm has been created to determine an RFI index based on the correlation of these fluctuations in multiple GNSS tracks [9]. The index is proportional to the RFI strength. With this release, the RFI index is included in the podTc2, scnPhs, scn1c2, and scnLv2 data products.

However, Cal/Val team analysis determined that the RFI index did not always clearly correlate with corruption of the on-board S4 index and related scintillation products. As a result, a separate quality control flag was developed that identifies when S4 (and the high-

Table 1: File Types Included in Data Release

File Type	Comment
podTc2	• Low rate absolute TEC, SNR, and S4 • RFI index and RFI QC flag included • S4 time tag adjusted by 5 seconds
scnPhs	• High-rate phase and amplitude data • RFI index and RFI QC flag
scn1c2	• S4 amplitude index and auxillary data computed in near real-time on-board the LEO satellite by TGRS receiver. • RFI index and RFI QC flag
scnLv2	• Scintillation amplitude (S4) and scintillation phase ($\sigma\phi$) computed on ground from high-rate phase and amplitude data (scnPhs) • RFI index and RFI QC flag

rate data S4 is derived from) are corrupted by RFI. This flag can be used to exclude RFI corrupted data from studies of ionospheric scintillation. The flag is set if S4 is simultaneously elevated above the sensor noise floor on multiple zenith hemisphere tracks and on at least one occulting track. With this release, this RFI flag is also included in the podTc2, scnPhs, scn1c2, and scnLv2 data products. Table 1 lists the file types that are new or have been updated to contain new information associated with TGRS scintillation observations.

2.2 IVM Temperature, and Composition Measurements

The IVM ion temperature and composition observations that are being released have been validated through comparisons with the Jicamarca Radio Observatory (JRO) [10] during overflights in 2020. These comparisons (Figures 4 and 5) are adequate to establish the accuracy of these products as better than 20%. Temperature and composition accuracies may actually be better than this (F7C2 performance objectives were 10% and 5%, respectively), but natural geophysical variability and contamination of the JRO observations by orbital debris resulted in higher than expected uncertainties in the truth dataset.

2.3 IVM Drift Measurements

The IVM FM1 early-mission drifts that are being released are provisional in nature because future refinement of the drift bias offsets is likely and some contamination by photo-electron effects is not yet corrected. The discussion below describes considerations that should be made by scientists making use of these data.

The ion drift is derived from the IVM measurement of the flow energy of the ions along the look direction of the sensor and by measurement of the angle of arrival of the ion flow

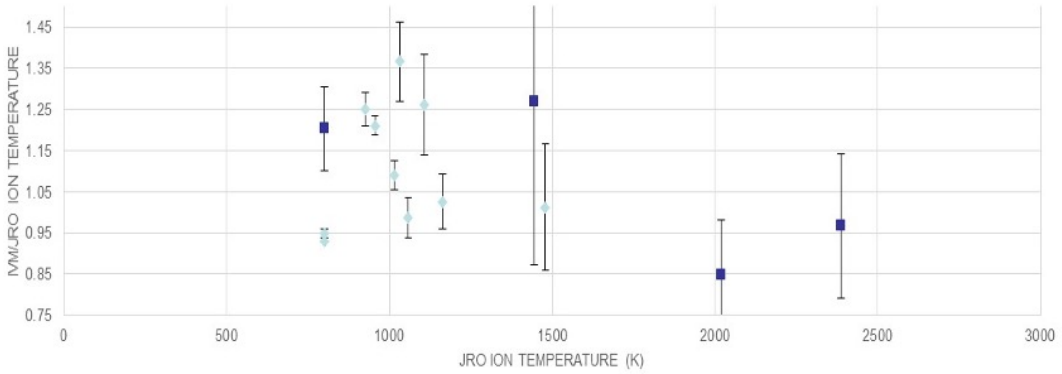

Figure 4: IVM/JRO temperature ratios for JRO overflights. Dark blue squares represent IVM sensors on F7C2 satellites at 720 km altitude (prior to final orbit lowering). Light blue diamonds represent IVM sensors on F7C2 satellites at 550km altitude. Error bars reflect uncertainties in the JRO observations.

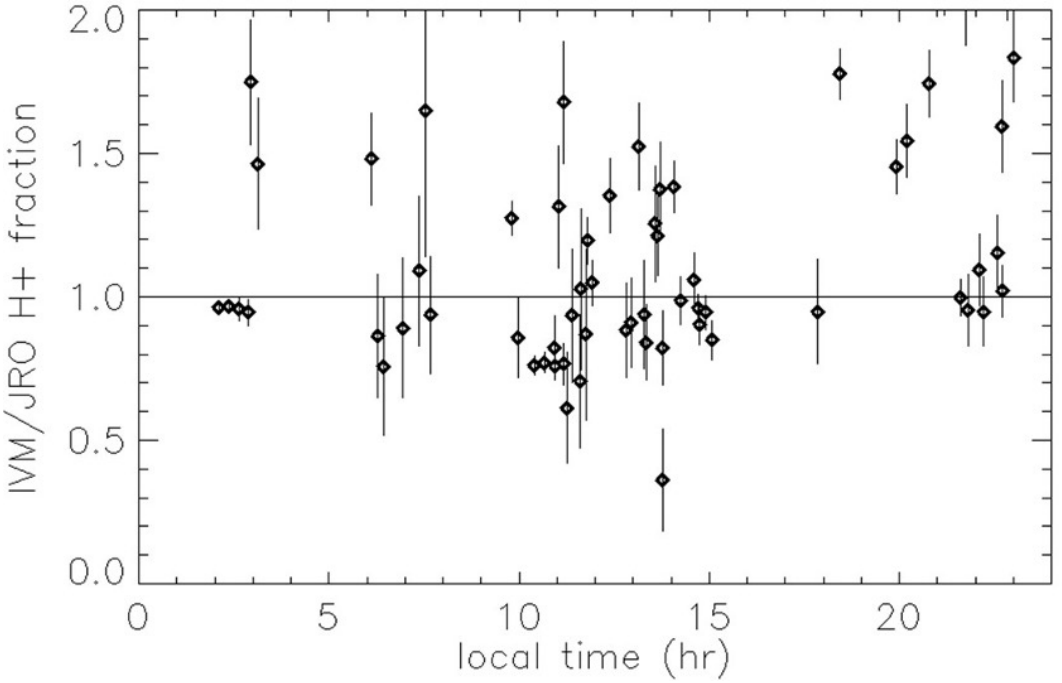

Figure 5: IVM/JRO hydrogen ion fraction ratios for JRO overflights. Error bars reflect the combined uncertainties of the JRO and IVM observations but are dominated by JRO uncertainties.

with respect the look direction of the sensor [8].

It should be recognized that measurement of the ion flow energy and the ion flow arrival angle are extremely sensitive to the sensor look direction and the electrostatic environment of the spacecraft. Many of the factors affecting these attributes of the spacecraft are unknown before launch and may change due to changing conditions during normal operations of the instrument. These factors may produce systematic offsets in the determination of flow energy

and flow angle that may occur over a range of spatial scales that are dependent on the prevailing environment. Changes in environmental conditions that change the fidelity with which the plasma drift can be determined cannot always be identified on a point-by-point basis by deviations from expected behavior. Further, the time scales of some deviations do not allow their removal based on long-term behavior over a typical repetition cycle equivalent to the precession period of the orbit.

The use of plasma drift data for statistical or event analysis should therefore be preceded by an examination of the global behavior of the drift over a temporal period of a few days surrounding a given target time.

2.3.1 Data Content

Figure 6 shows an example of one day of data from FM1. The meridional and zonal drift for each orbit are shown from the originally measured ion drift components in the spacecraft reference frame. For the purposes of explanation, the original time series data have been smoothed over 15-points (14 second window) with outliers exceeding the median value by more than 50 m/s removed. The velocities show a repeatable variation in local time but a variance about the mean value that is comparable to the mean value. This behavior is in accord with previous observations of plasma drifts from a single location [12]. Days for which the local time variation is not repetitive within a variance approximately the same as the peak-to-peak daily variation, should be reviewed carefully. Such variations during a single day may occur during storm times but the data should be examined for the presence of systematic offsets that do not evolve in time.

This display additionally serves to indicate several boundaries in the data across which the data should be examined.

Note first that regions where the O+ density is less that $10^3 cm^{-3}$ may suffer from signal drop-out or poor signal to noise ratio that causes the drift to display erroneously large values. In most cases these points are removed but some may still be present in the data. In the region between sunrise (≈0600 LT) and 1100 LT solar radiation is incident in the internal surfaces of the sensors. Scattered secondary electron emissions from the collector and the grids can lead to contaminated signals during this period. Contamination can be recognized by unusually large temporal gradients in the drift signal that appear in the meridional drift. Drifts during this period should be excluded from consideration at this time.

In Figure 6, the large-scale zonal and meridional drifts are smoothed over spatial scales of about 100 km corresponding to about 5 minutes in local time. In the post sunset region, the appearance of plasma density irregularities in which the embedded drifts may be large, an average value may be inappropriate to describe the prevailing physical configuration. In such

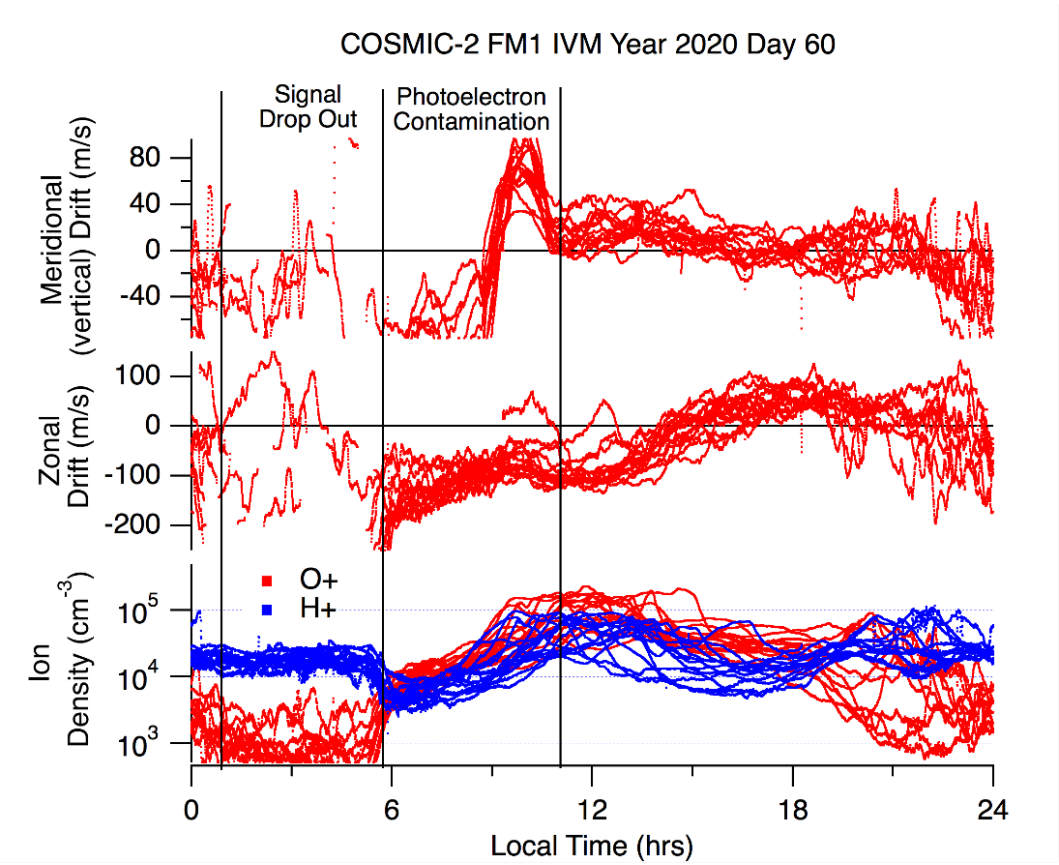

Figure 6: Single day data from the IVM show repetitive passes in local time that traverse different longitudes.

cases the original drift values reported at 1Hz should be treated with alternative analysis techniques that remove the signals from irregularity regions or otherwise account for their presence.

2.3.2 Validation

Measurements of IVM drift for FM1 from August 2019 through June 2020 are being provided to the research community as part of this data release. This time window corresponds to a period when FM1 was operating in its final orbit altitude of 550 km. As described below, these data have been evaluated using observations collected at the JRO [10] and model output from the WACCM-X model [11]. IVM drift observations from other spacecraft remain to be validated.

The plasma drift is originally measured in the spacecraft reference frame and is subject to offsets due to uncertainties in mounting and pointing direction and due to changes in the electrostatic environment around the spacecraft. Offsets to each of the s/c derived velocity components are determined by demanding that the vertical drift at the magnetic equator

reverse from outward to inward across the dusk terminator and that the meridional $\vec{E} \times \vec{B}$ drifts be approximately conjugate at magnetic latitudes of 10°N and 10°S.

Figure 7 shows the meridional (vertical $\vec{E} \times \vec{B}$) drift at the magnetic equator extracted from the F7C2 FM1 data and compared to climatological variations extracted from observations at the JRO radar and utilizing the WACCM-X model. The WACCM-X results were interpolated in time and space to the location of the F7C2 observations. These different data sources compare favorably with respect to large scale features and differ in detail due to geophysical variability that is known to have a magnitude comparable to the local time peak to peak variation. Ion drifts from these three sources compare well in the local time regions previously identified where reliable data from F7C2 are available.

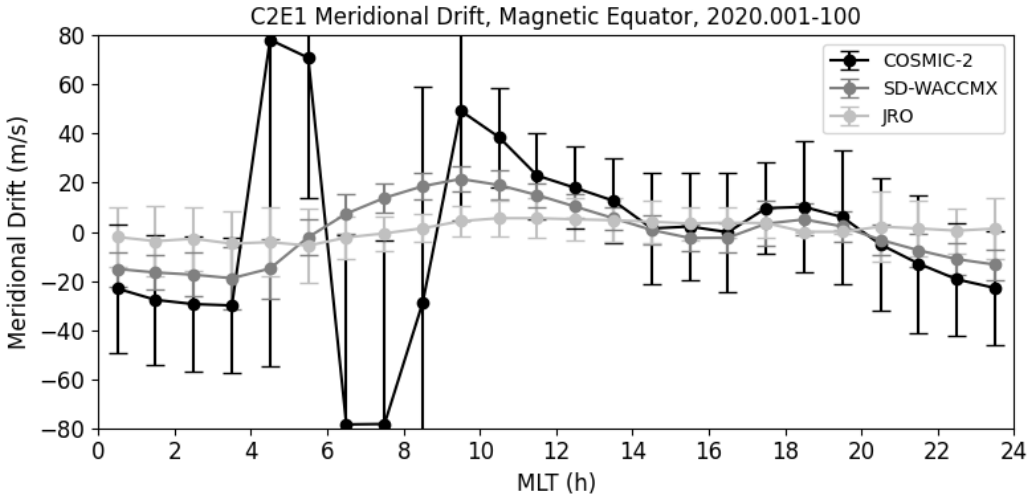

Figure 7: Comparison of meridional (vertical $\vec{E} \times \vec{B}$) ion drift at the magnetic equator, derived from F7C2 FM1, the JRO, and derived from WAACM-X model.

Zonal drifts from these same data sources are shown in Figure 8. Shown here are local time variations at the magnetic equator derived from F7C2 data, from JRO radar observations and from the WACCM-X model. We note that at this time the derivation of offsets in the native drifts measured by F7C2 does not incorporate any consideration of the behavior of the zonal drifts. Comparison of the zonal ion drifts resulting from the offset derivations for the meridional drift show that systematic differences of order 30-40 m/s appear between the F7C2 outputs and the climatology described by available measurements at Jicamarca and the output of the WACCM-X model.

Figure 9 expands upon the behavior of the ion drifts derived by F7C2 by comparing the measurements with the climatology extracted from the WACCM-X model at ±15° magnetic latitude. It is clear that this comparison suggests the additional refinement of the offsets may be required to conform more closely to the expected climatology. However, we also

note that the measurements suggest that a variation in the zonal drift with apex height may exist in the measurements that is not reproduced in the model. It is emphasized that measurements at conjugate locations for the same local time are taken at different epochs during the mission. Thus, a strict enforcement of equality at these locations is not feasible. However, further investigation of this data set to enforce reasonable assumptions of magnetic conjugacy for both meridional and zonal ion drifts may lead to refined offsets that will appear in subsequent updates to this dataset.

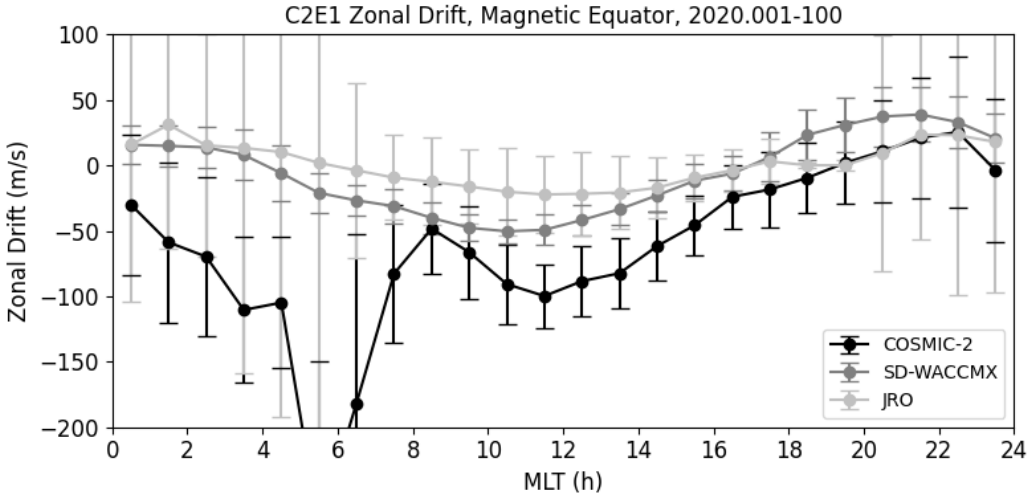

Figure 8: Comparison of zonal (+ve east) ion drift at the magnetic equator derived from F7C2 FM1, the JRO, and derived from WACCM-X model.

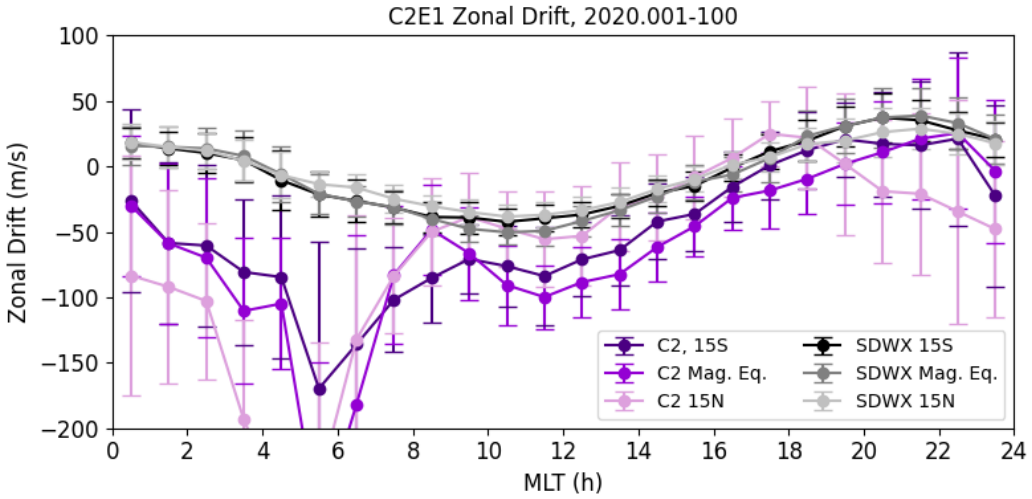

Figure 9: Comparison of zonal drifts from F7C2 FM1 and WACCM-X at magnetic equator and ±15° magnetic latitude.

3 Data Caveats

We note the following caveats to data users:

- Prior releases of TEC data (podTc2 files) contained provisional on-board S4 measurements. As part of the verification process, it has been determined that the S4 data were being reported with a time tag corresponding to the end of the 10 second interval over which the S4 measurement was computed. These time tags are now corrected to correspond to the middle of the 10 second interval and are therefore adjusted in time by -5 seconds.

4 Path Forward

The F7C2 DPC will initially provide TGRS and IVM temperature and composition products for the data types described in this release memo starting on March 16, 2022. Daily products will be made available from this date moving forward. Historical data, stretching back to earlier periods of the mission, require significant reprocessing and are anticipated to be released later in 2022. However, provisional release of IVM ion drifts from August 2019 thru June 2020 IVM will occur on March 16, 2022.

It is expected that additional IVM early mission (prior to June 2020) drift measurements from periods after FM2 and FM4 were lowered to their 550 km orbit altitude will be released later in 2022. Currently there is no timeline when data collected from spacecraft at the orbit insertion orbit altitude of 720 km might be released, but it should be noted that drift measurements made at this altitude are generally poor because of the dominance of light ions. For data collected at the 550 km altitude, the Cal/Val team is currently investigating an issue pertaining to anomalous across-track drift observations that began in June 2020. The Cal/Val team is exploring alternative options for IVM drift data release, including the potential to release in-track drift observations without corresponding cross-track observations. Currently there is not a definite timetable for release of additional drift data.

With the exception of the early mission FM1 IVM drifts, all space weather data products described in this memo are expected to be released on a daily basis. Operational constraints may, however, cause occasional delays. While not anticipated, if significant processing changes impacting product quality are made, we will increment the release version, make a corresponding data download area subdirectory, and provide release notes describing the changes.

5 Links

- F7C2 space weather data download
  https://www.cosmic.ucar.edu/what-we-do/cosmic-2/data/
  https://tacc.cwb.gov.tw/v2/download.html
- COSMIC Data Analysis and Archive Center
  https://www.cosmic.ucar.edu/what-we-do/data-processing-center/
- Taiwan Analysis Center for COSMIC
  https://tacc.cwb.gov.tw
- CDAAC user support forum
  https://groups.google.com/a/ucar.edu/forum/#!forum/cdaac-users
- Algorithms for inverting radio occultation signals in the ionosphere
  https://cdaac-www.cosmic.ucar.edu/cdaac/doc/documents/gmrion.pdf
- podTc2/podTc2 format
  https://cdaac-www.cosmic.ucar.edu/cdaac/cgi_bin/fileFormats.cgi?type=podTc2
  https://tacc.cwb.gov.tw/v2/en/fileformat.html#podTc2
- scn1c2/scn1c2 format
  https://cdaac-www.cosmic.ucar.edu/cdaac/cgi_bin/fileFormats.cgi?type=scn1c2
  https://tacc.cwb.gov.tw/v2/en/fileformat.html#scn1c2
- scnPhs/scnPhs format
  https://cdaac-www.cosmic.ucar.edu/cdaac/cgi_bin/fileFormats.cgi?type=scnPhs
  https://tacc.cwb.gov.tw/v2/en/fileformat.html#scnPhs
- scnLv2/scnLv2 format
  https://cdaac-www.cosmic.ucar.edu/cdaac/cgi_bin/fileFormats.cgi?type=scnLv2
  https://tacc.cwb.gov.tw/v2/en/fileformat.html#scnLv2

References

[1] Braun et al., *Performance of the FORMOSAT-7/COSMIC-2 Tri-GNSS Radio Occultation System (TGRS) Instrument During Early Orbit Operations for Space Weather Applications*, Fall AGU, San Francisco, USA, December, 2019.

[2] Straus et al., *Validation of COSMIC-2 Space Weather Science Products*, AMS Annual Meeting, USA, January, 2020.

[3] Liu et al., *FORMOSAT-7/COSMIC-2 Mission and Preliminary Results*, Fall AGU, San Francisco, USA, December, 2019.

[4] *Space Weather Data Release 1* `https://data.cosmic.ucar.edu/gnss-ro/cosmic2/provisional/spaceWeather/F7C2_SpWx_Provisional_Data_Release_1.pdf`

[5] *Space Weather Data Release 2* `https://data.cosmic.ucar.edu/gnss-ro/cosmic2/nrt/F7C2_SpWx_GPS_Absolute_TEC_Data_Release_Memo.pdf`

[6] *Space Weather Data Release 3* `https://data.cosmic.ucar.edu/gnss-ro/cosmic2/nrt/F7C2_SpWx_GLO_Absolute_TEC_Data_Release_Memo.pdf`

[7] *Space Weather Data Release 4* `https://data.cosmic.ucar.edu/gnss-ro/cosmic2/nrt/F7C2_SpWx_IVM_Density_Data_Release_Memo.pdf`

[8] Heelis, R. A., R. A. Stoneback, M. D. Perdue, M. D. Depew, W. A. Morgan, M. W. Mankey, C. R. Lippincott and L. L. Harmon and B. J. Holt, *Ion Velocity Measurements for the Ionospheric Connections Explorer*, Space Science Reviews, doi:10.1007/s11214-017-0383-3,2017.

[9] T.M. Roberts, T. Meehan, J. Tien, and L. Young, *Detection and Localization of Terrestrial L-Band RFI with GNSS Receivers*, Trans. Geosci. Remote Sens., doi:10.1109/TGRS.2021.3109524.

[10] D. L. Hysell, J. L. Chau and M. A. Milla, *The Jicamarca phased-array radar*, IEEE International Symposium on Phased Array Systems and Technology, 2013, pp. 669-675 doi: 10.1109/ARRAY.2013.6731910

[11] Liu, H.-L., Bardeen, C. G., Foster, B. T., Lauritzen, P., Liu, J., Lu, G., Marsh D. R., Maute A., McInerney J. M., Pedatella N. M., Qian, L., Richmond A. D., Roble R. G., Solomon S. C., Vitt F. M., Wang, W. *Development and validation of the Whole Atmosphere Community Climate Model with thermosphere and ionosphere extension (WACCM-X 2.0)*, Journal of Advances in Modeling Earth Systems, 10, doi: 10.1002/2017MS001232

[12] Fejer, B. G., Jensen, J. W., and Su, S.-Y., *Quiet time equatorial F region vertical plasma drift model derived from ROCSAT-1 observations*, J. Geophys. Res., 113, A05304, doi:10.1029/2007JA012801